

Deconvolution-Interpolation Gridding (DING): Accurate Reconstruction for Arbitrary k -Space Trajectories

Refaat E. Gabr,^{1,2*} Pelin Aksit,³ Paul A. Bottomley,^{1,4} Abou-Bakr M. Youssef,² and Yasser M. Kadah²

A simple iterative algorithm, termed deconvolution-interpolation gridding (DING), is presented to address the problem of reconstructing images from arbitrarily-sampled k -space. The new algorithm solves a sparse system of linear equations that is equivalent to a deconvolution of the k -space with a small window. The deconvolution operation results in increased reconstruction accuracy without grid subsampling, at some cost to computational load. By avoiding grid oversampling, the new solution saves memory, which is critical for 3D trajectories. The DING algorithm does not require the calculation of a sampling density compensation function, which is often problematic. DING's sparse linear system is inverted efficiently using the conjugate gradient (CG) method. The reconstruction of the gridding system matrix is simple and fast, and no regularization is needed. This feature renders DING suitable for situations where the k -space trajectory is changed often or is not known a priori, such as when patient motion occurs during the scan. DING was compared with conventional gridding and an iterative reconstruction method in computer simulations and in vivo spiral MRI experiments. The results demonstrate a stable performance and reduced root mean square (RMS) error for DING in different k -space trajectories. Magn Reson Med 56: 1182–1191, 2006. © 2006 Wiley-Liss, Inc.

Key words: gridding; nonuniform sampling; density compensation function; deconvolution-interpolation; arbitrary trajectories

The reconstruction of images from nonuniform samples of their spatial frequency domain (k -space) is an important problem in fields as diverse as computed imaging and radioastronomy. A convolution-interpolation algorithm known as the “gridding algorithm” is widely used to reconstruct images from such data. Basically, this conventional gridding algorithm (1,2) convolves the nonuniform samples with a small-width window, and samples the result onto a rectilinear grid. It consists of the following four steps: First, the nonuniform samples are compensated for the nonuniform sampling density in k -space by multiplication with a weighting function the density compen-

sation function (DCF), which has small values in areas of high sampling density and large values in sparsely sampled areas. Second, the density-compensated data are interpolated to a uniform grid using a small convolution window. Third, the data are Fourier transformed (FT) into the image domain. Fourth, apodization caused by the convolution step is compensated for by dividing the result by the FT of the convolution window.

The conventional gridding algorithm is efficient and stable because the convolution step has a smoothing effect, but it has been shown to be non-optimal and artifact-prone (3,4). Density compensation is necessary to adequately approximate the convolution operation (3), and several studies have attempted to determine the optimum DCF (2,5,6). The final step in the conventional gridding algorithm, which compensates for the convolution roll-off, results in large signal at the image periphery (wings) due to the side lobes of the convolution window, and the aliasing caused by the sampling process. Sampling the result of the convolution onto a finer grid reduces aliasing and wing artifacts in the reconstructed image. A twofold subsampling (“twice-finer” grid) is commonly used to achieve acceptable image quality.

Other methods used to overcome limitations in the conventional gridding algorithm commonly exploit the relationship between the acquired k -space samples and their rectilinear counterparts, as given by the standard sinc-function interpolation of the sampling theorem (7). This relationship is strictly valid only if the signal is of infinite length in k -space, but it does provide a good approximation if k -space coverage is large. Discrete sampling of the interpolation results in a linear system with a dense sinc-interpolation matrix, the inversion of which results in the uniform resampling (URS) solution (8). While inverting the sinc-coefficients matrix is practical for one-dimensional (1D) signals, it becomes impractical for higher dimensions due to the tremendous matrix size, except for special cases (9). Nevertheless, the conventional gridding algorithm has been shown to be an approximation of the URS solution, and an optimal DCF that minimizes the difference between the gridding and the URS solution is obtained with matrix approximation techniques for structured matrices (7). However, these techniques are computationally exhaustive.

The block URS (BURS) method is an approximation to the URS solution that aims to reduce computational effort (8). A small block of the sinc-matrix around each grid point is isolated and inverted to obtain a spatially varying convolution window. Attention to regularization is critical, and poor estimates are reported for Lissajous k -space trajectories (9–11). The computation required to reconstruct the gridding matrix is still huge, although it only has

¹Department of Electrical and Computer Engineering, Johns Hopkins University, Baltimore, Maryland, USA.

²Department of Biomedical Engineering and Systems, Cairo University, Giza, Egypt.

³Global Applied Science Laboratory, GE Healthcare, Waukesha, Wisconsin, USA.

⁴Division of MR Research, Department of Radiology, Johns Hopkins University, Baltimore, Maryland, USA.

Grant sponsor: National Institutes of Health; Grant numbers: R01 RR15396; R01-HL61695.

*Correspondence to: Refaat Gabr, Division of MR Research, JHOC 4240, Department of Radiology and Radiological Science, Johns Hopkins University, 601 N. Caroline St., Baltimore, MD 21287. E-mail: gabr@jhu.edu

Received 9 February 2006; revised 27 July 2006; accepted 18 August 2006. DOI 10.1002/mrm.21095

Published online 6 November 2006 in Wiley InterScience (www.interscience.wiley.com).

to be done once for a given trajectory. Nonuniform fast FT (NUFFT) techniques have also been utilized to provide spatially varying convolutions that minimize measures of the approximation error (12–15). In another approach, a model of the imaged object is assumed and is used to derive an optimal spatially-varying interpolation kernel (16).

Nonuniform sampling can be formulated as a continuous-to-discrete mapping through the FT operator. This system can be inverted using singular value decomposition (SVD), and offers the advantage of arbitrary sampling in the image domain (5). To avoid the huge computational load and regularization problems, previous studies solved a discrete version of the same formulation iteratively using the conjugate gradient (CG) method, whereby each iteration of the solution involves a forward and an inverse gridding operation (4,17). This solution has been also employed to reconstruct sensitivity-encoded (SENSE) images from arbitrary trajectories (18). In the rest of this paper we refer to this iterative inversion of the Fourier encoding system using CG as “F-CG.” Although density compensation is not needed in the gridding operation in F-CG, density compensation has been suggested as a preconditioner to the CG matrix to reduce the number of iterations (18). The same formulation of the problem can be solved in a different way by noting that the dense Fourier exponential matrix can be converted into a sparse form by the application of a compacting transform to the rows of this matrix. The resulting sparse linear system can then be efficiently solved using the CG method (19).

A characteristic of all of these methods is that they require intensive calculations to invert or construct a gridding matrix, and in many cases careful regularization is essential in order to maintain stability and avoid noise amplification. The truncations and approximations made by many of these methods (5,8,19) influence the accuracy of the solution and introduce artifacts that are not well characterized.

In this work we introduce a new solution to the gridding problem that solves a more accurate yet simple formulation of the problem. Instead of the convolution-interpolation operation used in the conventional gridding algorithm that depends on the DCF used, an iterative deconvolution-interpolation gridding (DING) algorithm is implemented. DING utilizes the CG method to solve a sparse system of linear equations in a manner equivalent to a deconvolution operation. The theory and implementation of DING for the reconstruction of simulated data with spiral and random k -space trajectories and real spiral MRI data are presented, and its performance is quantified relative to the conventional gridding and F-CG methods.

THEORY

Let $M(\mathbf{k})$ be the continuous FT of the object to be imaged as a function of the continuous k -space position \mathbf{k} , and $S(\mathbf{k})$ be the nonuniform sampling function that consists of a series of impulses at required sampling locations, such that:

$$S(\mathbf{k}) = \sum_{j=1}^L \delta(\mathbf{k} - \kappa_j). \quad [1]$$

where L is the number of data points, $\{\kappa_j\}_{j=1:L}$ are arbitrary sampling locations, and $\delta(\cdot)$ is the Dirac delta function. The sampled k -space $M_s(\mathbf{k})$ is thus given by $M_s(\mathbf{k}) = M(\mathbf{k})S(\mathbf{k})$. The sampling theorem states that $M(\mathbf{k})$ can be exactly reconstructed from the discrete samples on a uniform grid via an infinite sinc-function interpolation, provided that the Nyquist criterion is satisfied by the sampling grid. Assuming that the k -space is well sampled by N samples such that the Nyquist criterion is satisfied and the N samples cover the whole k -space, this relationship can be written as

$$M(\mathbf{k}) = \sum_{n=1}^N M(k_n) \text{sinc}(|\mathbf{k} - k_n|), \quad [2]$$

where $\{k_n\}_{n=1:N}$ are the rectilinear grid points, and the modulus term measures distance. Calculating Eq. [2] at the L nonuniform samples $\{\kappa_j\}_{j=1:L}$ and stacking the non-rectilinear samples $\{M(\kappa_j)\}_{j=1:L}$ and their rectilinear counterparts $\{M(k_n)\}_{n=1:N}$ in column vectors \mathbf{m}_s and \mathbf{m}_r respectively, a compact matrix form for this relation is:

$$\mathbf{m}_s = \mathbf{A}\mathbf{m}_r. \quad [3]$$

where \mathbf{A} is a dense matrix containing the sinc interpolation coefficients, $\mathbf{A}_{jn} = \text{sinc}(|\kappa_j - k_n|)$. Because Eq. [3] is a convolution operation, inverting this equation to get \mathbf{m}_r is essentially an algebraic inverse-filtering, or deconvolution (20), of the k -space data with the sinc function. Solving Eq. [3] is impractical because of the prohibitively large size of \mathbf{A} .

To improve the efficiency of the solution, we replace the infinite sinc function with a small window $C(\mathbf{k})$ of finite support in a manner similar to conventional gridding (1). Defining $D(\mathbf{k})$ to be the result of the deconvolution of $M(\mathbf{k})$ and $C(\mathbf{k})$, we replace the formulation in Eq. [2] with

$$M(\mathbf{k}) = D(\mathbf{k}) * C(\mathbf{k}) = \int D(\mathbf{k}') C(|\mathbf{k} - \mathbf{k}'|) d\mathbf{k}' \quad [4]$$

where $*$ denotes convolution. The solution of Eq. [4] is calculated on a rectilinear grid, yielding

$$D_r(\mathbf{k}) = (M(\mathbf{k}) *^{-1} C(\mathbf{k})) III(\mathbf{k}) \quad [5]$$

where $(*^{-1})$ denotes deconvolution, and $D_r(\mathbf{k})$ is a uniformly sampled version of $D(\mathbf{k})$, $D_r(\mathbf{k}) = D(\mathbf{k}) III(\mathbf{k})$, where $III(\mathbf{k}) = \sum_{n=1}^N \delta(\mathbf{k} - k_n)$ is the grid sampling function (i.e., the Shah function). In the spatial domain, this is equivalent to

$$d_r(\mathbf{r}) = \frac{m(\mathbf{r})}{c(\mathbf{r})} * III(\mathbf{r}) \quad [6]$$

where the lowercase variables are the inverse-FT of the corresponding uppercase variables, and \mathbf{r} is the position variable in the image space. The relationship between $D_r(\mathbf{k})$ and $M(\mathbf{k})$ is easily inferred from the corresponding inverse Fourier transforms, $d_r(\mathbf{r})$, and $m(\mathbf{r})$. The reconstructed image $d_r(\mathbf{r})$ and the desired image $m(\mathbf{r})$ are related

by the modulating function $1/c(\mathbf{r})$ resulting from the deconvolution operation, plus the aliasing introduced by the Shah function. The intensity modulation effect can be simply eliminated by multiplying the image in the central part by $c(\mathbf{r})$ and truncating the result to the field-of-view (FOV). To obtain the final image estimate $m_{est}(\mathbf{r})$:

$$m_{est}(\mathbf{r}) = \left[\frac{m(\mathbf{r})}{c(\mathbf{r})} * III(\mathbf{r}) \right] c(\mathbf{r}) \Pi_{FOV}(\mathbf{r}), \quad [7]$$

where $\Pi_{FOV}(\cdot)$ is the *Rect* function that truncates the object to the FOV.

An implementation of DING will first solve a discretized version of Eq. [4], with $M(\mathbf{k})$ measured only at the L points $\{\kappa_j\}_{j=1:L}$, to form the sparse system:

$$M(\kappa_j) \approx \sum_n D(k_n) C(|\kappa_j - k_n|) \quad j = 1:L \quad n = 1:N. \quad [8]$$

One can make the approximation in Eq. [8] arbitrarily accurate by choosing a finer uniform grid. Nevertheless, for a regular grid the approximation is quite accurate because D is sampled on a uniform grid and no DCF is needed. Note that in order to avoid aliasing in D when solving Eq. [8], the Nyquist criterion must be satisfied by the nonuniform sampling function $S(\mathbf{k})$. The discretized system is compactly written as

$$\mathbf{m}_s = \mathbf{C} \mathbf{d}_r, \quad [9]$$

where \mathbf{C} is the $L \times N$ interpolation matrix with $C_{jn} = C(|\kappa_j - k_n|)$, and \mathbf{d}_r is a vector of the stacked uniform samples of D . Thus, the steps of the DING solution are as follows: 1) solve Eq. [9] for \mathbf{d}_r using the CG method, 2) perform an inverse-FT into the image domain, and 3) multiply the result by $c(\mathbf{r})$ to compensate for the effect of the deconvolution. The conventional gridding algorithm and DING are illustrated in Fig. 1.

Since \mathbf{C} is a sparse matrix, the linear system in Eq. [9] is efficiently inverted using the CG method. The CG method optimizes the solution of a symmetric positive-definite system by removing the error components in independent directions that span the space of the solution (21). It is well suited for sparse linear systems because each iteration involves only a single matrix-vector multiplication, and minimal low-cost inner-product operations. Here the method is applied to solve the normal equations of Eq. [9], where the system matrix $\mathbf{C}^T \mathbf{C}$ is symmetric and positive definite.

A Kaiser-Bessel window is used as the interpolating window, $C(\mathbf{k})$. The Kaiser-Bessel window has small side-lobe energy outside the passband, and is a good approximation to the optimal zero-order prolate-spheroidal wave function of the first kind, which has the least amount of side-lobe energy (2). The optimum window parameter, β , is set by the criterion of Eq. [12] of Ref. 2, with the variables $c(\mathbf{r})$ and $1/c(\mathbf{r})$ interchanged to reflect the use of a deconvolution operation for interpolation instead of a convolution. The measure to be minimized, E , is thus given by

$$E = \frac{\int_{\mathbf{r} \in FOV} \left| \frac{[\Pi(\mathbf{r})c(\mathbf{r})]^* III(\mathbf{r})}{c(\mathbf{r})} \right|^2 d\mathbf{r}}{\int_{\mathbf{r}} \left| \frac{[\Pi(\mathbf{r})c(\mathbf{r})]^* III(\mathbf{r})}{c(\mathbf{r})} \right|^2 d\mathbf{r}}. \quad [10]$$

This criterion minimizes the relative amount of the aliasing energy, including the effect of the deconvolution correction. Regularization is required during the calculation of β when dividing by very small numbers in the window tail (numbers less than 0.01 for a normalized window are excluded from the calculation). Optimal values for β are listed in Table 1.

MATERIALS AND METHODS

We evaluated DING using simulated and real MRI data. To assess the performance of DING, we compared it with conventional gridding and F-CG. Conventional gridding was performed with a Kaiser-Bessel window of the same width as in DING, an optimal window parameter (2), and a twice-finer grid. The F-CG method was implemented according to Eq. [21] in Ref. 18. The matrix-vector multiplication in the CG iteration was performed by gridding and inverse gridding (17) operations with the same window parameters and grid subsampling factor as in conventional gridding. To investigate the effect of density compensation on the solution speed and noise amplification, we implemented two versions of F-CG (without and with density compensation turned on).

The simulated data are the result of sampling the continuous frequency domain of the Shepp Logan (SL) phantom (5) using a 32-interleave Archimedean spiral trajectory optimized for minimum readout time (22). Each interleave samples 4096 points and shares the central point. The SL phantom is shown in Fig. 2. All images are reconstructed to a 256×256 matrix. Noisy data are simulated by adding Gaussian white noise to both the real and imaginary parts of the ideal data. The mean of the noise is zero,

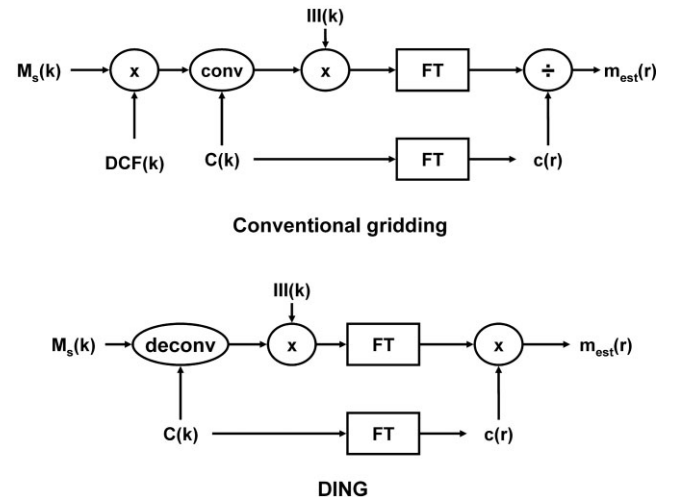


FIG. 1. The gridding algorithm of conventional gridding and DING.

Table 1
Optimal β Parameter for the Kaiser-Bessel Window Used in the DING Algorithm

Window width	1.5	2.0	2.5	3.0	3.5	4.0	4.5	5.0
β	5.56	5.52	5.50	5.49	5.52	5.48	5.48	4.82

and the standard deviation (SD) of the noise is equal to 20%, 40%, 60%, 80%, and 100% of the average magnitude of the original ideal k -space data (23). For conventional gridding and F-CG, a spiral analytical DCF is used: $\text{DCF}(\mathbf{k}_j) = \mathbf{g}_j \cdot \mathbf{k}_j$, where \mathbf{g}_j is the gradient vector at k -space position \mathbf{k}_j (24). A window size of three Cartesian grid units is used in all methods with optimal parameters. In DING and F-CG, the CG iterations are stopped either when the magnitude of the residual falls below 0.1% of the magnitude of \mathbf{m}_s , or the change in the residual magnitude falls below 1% of the initial change.

The reconstruction accuracy is quantified by calculating the root mean square (RMS) error between the reconstructed image and a reference image reconstructed from a uniformly sampled noiseless k -space of the phantom. The RMS error is normalized by the RMS of the reference image and is reported as a percentage. In simulations, the RMS error calculations employ a scalar multiplier in the reconstructed image to minimize the sum of the squared differences between the reconstructed image and the reference image. Note that this scaling does not result in any change in image contrast. To assess the stability of reconstruction, the signal-to-noise ratio (SNR) is calculated from two rectangular areas within the white ellipse and the background marked in Fig. 2 by the dark and bright rectangles, respectively. The SNR is defined as 0.655 times the ratio between the mean magnitude in the object region divided by the SD of the background region (25). The SNR

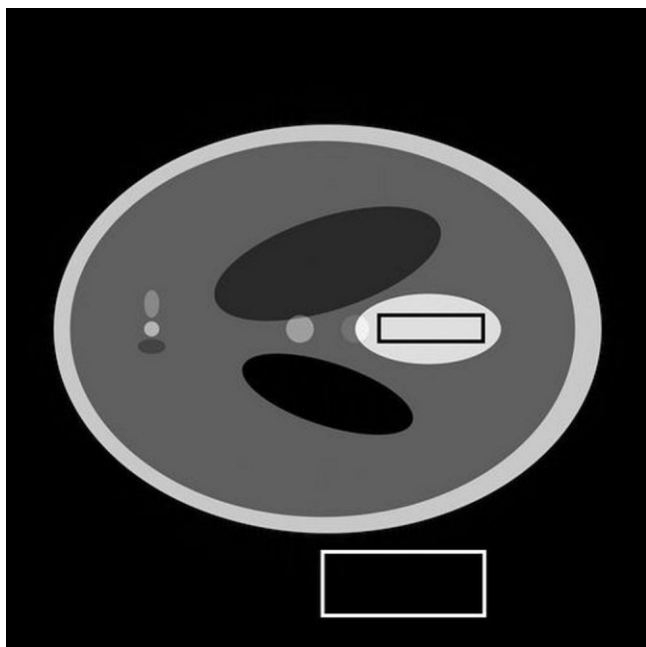


FIG. 2. Reference SL phantom. The SNR calculations are performed on the regions enclosed by the dark and bright rectangles as object and background, respectively.

measures how noise is amplified by each reconstruction technique, and when reconstruction artifacts are dominant, the SNR provides a reasonable measure of reconstruction accuracy.

To demonstrate performance for other k -space trajectories, we apply DING to the case of a randomly sampled k -space, where analytical expressions for the DCF do not exist. The simulation experiment is repeated for a random sampling pattern in which the k -space of the SL phantom is sampled using $256 \times 256 \times 4$ random samples generated from a uniform distribution in the desired k -space coverage. This large number of samples is sufficient to avoid undersampling problems. DING is applied in the same way as for the spiral trajectory, while for conventional gridding and F-CG, where no analytical DCF exists, the Voronoi cell area is used for density compensation (17,23). To avoid problems in calculating the Voronoi diagram at the periphery of the k -space, a sampling pattern set larger than the required k -space coverage is initially applied, followed by truncation after the Voronoi DCF is calculated.

For in vivo experiments, the same spiral trajectory used in the simulations (32-interleave Archimedean spiral trajectory with 4096 points per interleave) is used to acquire an axial brain gradient-echo image of a healthy volunteer on a 1.5T GE CV/i system (GE Healthcare, Waukesha, WI, USA). All human MRI studies are performed under an institutional review board-approved protocol. The scan parameters are as follows: FOV = 24 cm, slice thickness = 5 mm, TR/TE = 51/2.5 ms, flip angle = 60°, and NEX = 16. For DING, images are reconstructed onto a 380×380 grid zero-padded to 512×512 prior to FT. Conventional gridding and F-CG are implemented with the same spiral DCF as in the simulations, and a twice-finer grid. The same Kaiser-Bessel window with a width of three rectilinear grid points and optimal parameters is used.

While the spiral trajectory benefits from its uniform sampling pattern and optimal analytical DCF, problems arise when the trajectory undersamples the k -space and the Nyquist criterion is not satisfied, or the sampling uniformity is distorted. This occurs, for example, when variable-density trajectories designed to optimize speed (26) are used, or when the trajectory is distorted by motion during the scan (27). To test the performance of the three methods with the in vivo data in the case of nonuniform sampling, every eighth spiral interleave is removed from the trajectory, leaving 28 interleaves, and the collected data are reconstructed by DING as described above. For conventional gridding and F-CG, a Voronoi DCF is used for density correction to accommodate the irregular sampling pattern, instead of the analytical spiral DCF.

All of the methods are implemented offline on a PC (Intel Pentium M processor, 1.5 GHz, 512 MB of memory) operating on Microsoft Windows XP platform in MATLAB v6.5 (Mathworks, Natick, MA, USA).

RESULTS

Simulation

Figure 3 shows the reconstructed noiseless images of the SL phantom for the spiral k -space trajectory obtained with conventional gridding, the F-CG method, and DING. All images are visually indistinguishable, as also evidenced by the point spread function (PSF) profiles for the three methods shown in Fig. 4. Figure 5 shows the reconstructed images in the case of 60% noise. Again there is little perceptible difference between the conventional gridding, F-CG (without DCF), and DING images; however, the F-CG (with DCF) image shows more background artifacts. Note that using the preconditioning DCF is not SNR-optimal (18). Table 2 summarizes the RMS errors and the SNR values of the three reconstruction methods for different noise levels. The data show that better accuracy and SNR are achieved with DING.

For the random k -space trajectory, the DING and F-CG methods substantially outperform the conventional gridding algorithm in both accuracy and SNR (Table 3). It is obvious that the conventional gridding algorithm is unable to compensate for the varying sampling density, and the reconstruction error is dominant over noise. The noiseless images reconstructed by the three methods (Fig. 6) show intense sampling artifacts in the conventional gridding reconstruction, whereas these artifacts are not visible in the image reconstructed by DING or F-CG. This observation is reflected in the lower RMS error (Table 3). For this random trajectory, large tails are evident in the PSF of the conventional gridding algorithm, while a better PSF is obtained with F-CG, and a much better PSF results from using DING, as plotted in Fig. 7.

To show the convergence properties of the F-CG and DING methods, Fig. 8 shows the RMS error after each

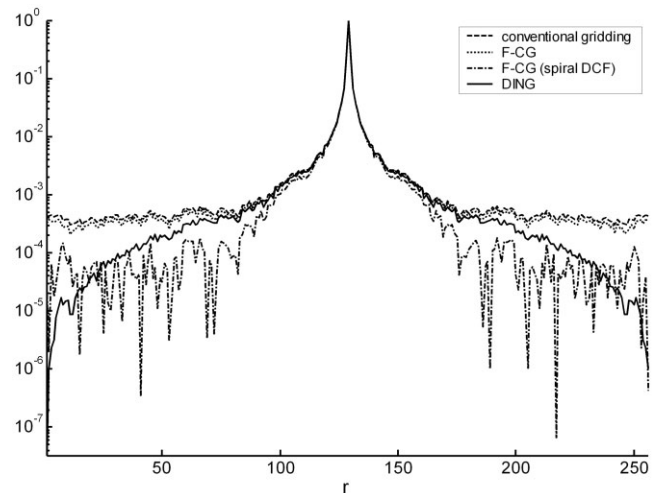


FIG. 4. PSF profile of conventional gridding, F-CG, and DING for the spiral trajectory. A logarithmic scale is used in the vertical axis.

iteration of the CG method for the random trajectory in the noiseless case. In both reconstruction methods the error drops sharply for the first few iterations and stabilizes after about 10–20 iterations. Fast convergence is evidenced for F-CG, and a faster convergence is achieved using DCF for preconditioning. However, higher RMS error is observed in the F-CG images in the presence of noise. On the other hand, although DING has a slower convergence, it exhibits better immunity toward noise (Fig. 8; Tables 2 and 3).

In Vivo Studies

Figure 9 shows in vivo spiral brain images reconstructed using the conventional gridding, F-CG, and DING meth-

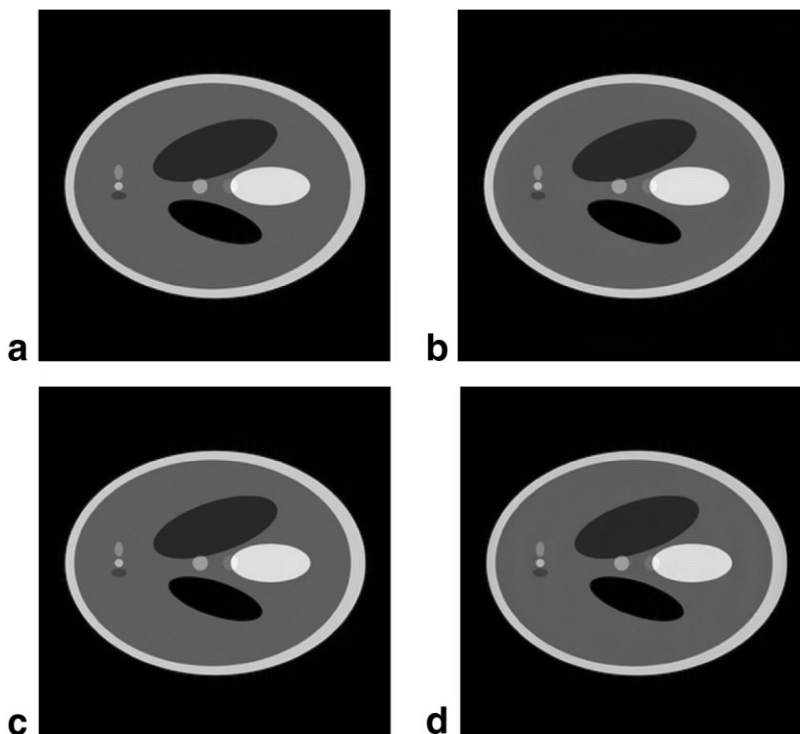
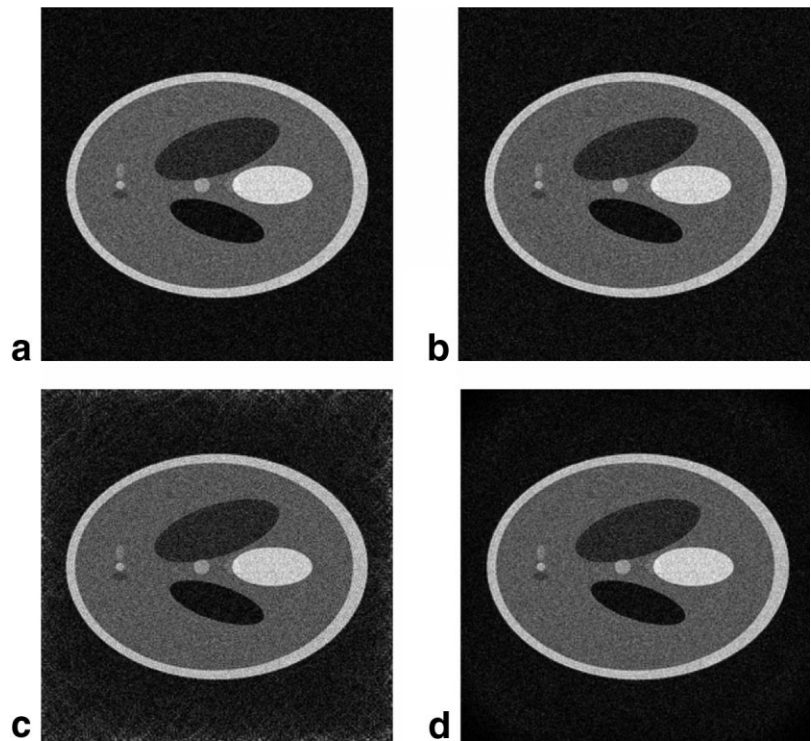


FIG. 3. Reconstructed images for simulated spiral sampling of the noiseless k -space of the SL phantom using conventional gridding (a), F-CG without (b) and with spiral DCF (c), and DING (d).

FIG. 5. Reconstructed images for simulated spiral sampling of the noisy k -space of the SL phantom (60% noise) using conventional gridding (a), F-CG without (b) and with spiral DCF (c), and DING (d).



ods. Both F-CG versions and DING converged in nine iterations. The locations of the object and background regions used for SNR measurement are indicated in black and white rectangles, respectively. The images recon-

structed by the three methods are of comparable quality. The image SNRs for conventional gridding, F-CG without and with DCF, and DING are 23.4, 22.1, 22.6, and 23.3, respectively, indicating a similar performance by conven-

Table 2
Comparison of the Performance of the Conventional Gridding, the F-CG, and the DING Algorithms for the Spiral Trajectory*

Noise level	Method (number of iterations)	RMS error (%)	SNR
0%	Gridding	2.6	N/A
	F-CG (7)	2.9	N/A
	F-CG + spiral DCF (2)	2.6	N/A
	DING (9)	4.9	N/A
20%	Gridding	7.4	47.9
	F-CG (7)	7.4	48.3
	F-CG + spiral DCF (13)	10.8	34.3
	DING (9)	7.0	56.0
40%	Gridding	14.1	24.1
	F-CG (7)	14.0	24.5
	F-CG + spiral DCF (16)	23.4	15.5
	DING (9)	11.4	28.1
60%	Gridding	20.1	16.1
	F-CG (7)	20.6	16.3
	F-CG + spiral DCF (16)	33.8	10.3
	DING (12)	17.1	17.2
80%	Gridding	27.2	12.1
	F-CG (7)	27.1	12.2
	F-CG + spiral DCF (16)	43.0	7.7
	DING (9)	21.7	13.3
100%	Gridding	33.1	9.7
	F-CG (8)	33.5	9.5
	F-CG + spiral DCF (16)	50.7	6.2
	DING (12)	28.4	9.8

*RMS errors are calculated as a percentage of the RMS of the reference image.

Table 3
Comparison of the Performance of the Conventional Gridding, the F-CG, and the DING Algorithms for the Random Trajectory*

Noise level	Method (number of iterations)	RMS error (%)	SNR
0%	Gridding	30.4	N/A
	F-CG (11)	0.5	N/A
	F-CG + Voronoi DCF (8)	0.82	N/A
	DING (13)	2.6	N/A
20%	Gridding	30.5	39.2
	F-CG (11)	2.8	106.0
	F-CG + Voronoi DCF (8)	3.0	112.8
	DING (13)	3.4	101.7
40%	Gridding	30.7	34.3
	F-CG (11)	5.6	58.4
	F-CG + Voronoi DCF (8)	6.1	54.7
	DING (13)	5.3	59.6
60%	Gridding	31.2	29.2
	F-CG (11)	8.5	39.2
	F-CG + Voronoi DCF (7)	9.1	36.8
	DING (13)	7.5	41.1
80%	Gridding	31.7	24.9
	F-CG (11)	11.4	29.5
	F-CG + Voronoi DCF (7)	12.1	27.7
	DING (13)	9.9	31.0
100%	Gridding	32.5	21.5
	F-CG (11)	14.2	23.6
	F-CG + Voronoi DCF (7)	15.2	22.2
	DING (13)	12.4	24.8

*RMS errors are calculated as a percentage of the RMS of the reference image.

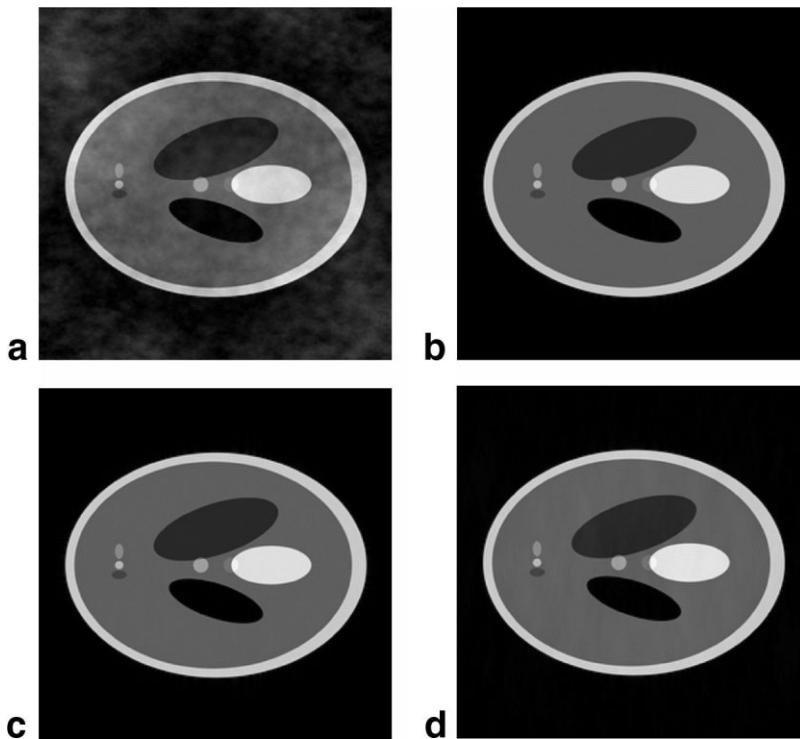


FIG. 6. Reconstructed images for simulated random sampling of the noiseless k -space of the SL phantom using conventional gridding (a), F-CG without (b) and with Voronoi DCF (c), and DING (d).

tional gridding and DING, and a slightly degraded performance by F-CG. With irregular sampling resulting from the removal of every eighth interleave, significant artifacts are evident in the conventional gridding image, which reduces the measured SNR in the same region to 8.0. The artifacts are much less noticeable in the F-CG without (nine iterations) and with DCF (nine iterations), and the DING (eight iterations) images, where the measured SNRs are 13.8, 15.5, and 16.8, respectively. These results show that conventional gridding fails to correctly adapt to this

irregular sampling even when the Voronoi DCF is used, while DING, although affected by the undersampling, fares best.

DISCUSSION

Our new DING algorithm enables images to be accurately reconstructed from arbitrarily-sampled k -space. This is achieved without grid subsampling, which is usually necessary when the conventional gridding algorithm is used.

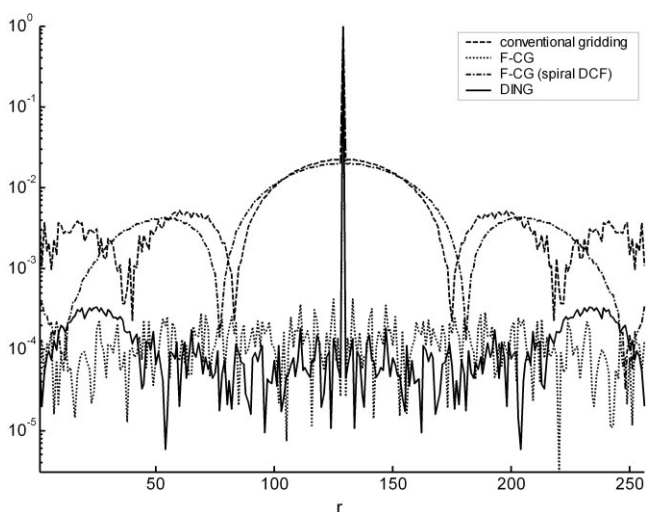


FIG. 7. PSF profile of the conventional gridding algorithm, F-CG, and DING for the random trajectory. A logarithmic scale is used in the vertical axis.

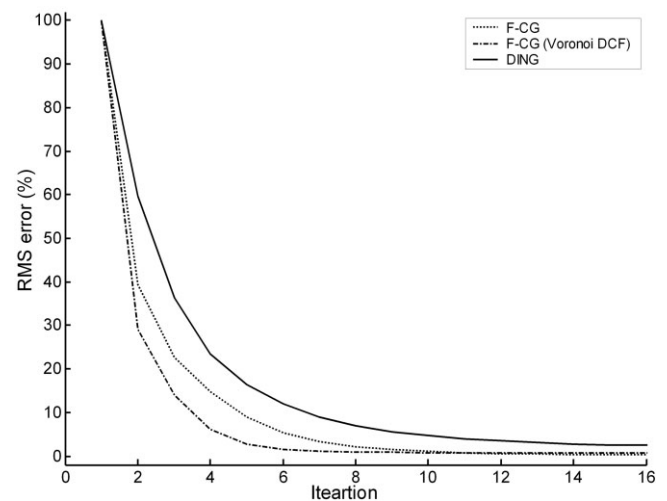


FIG. 8. The RMS error of F-CG and DING vs. the number of CG iterations for the simulated noiseless SL phantom and the random trajectory. Errors stabilize after approximately 15 iterations.

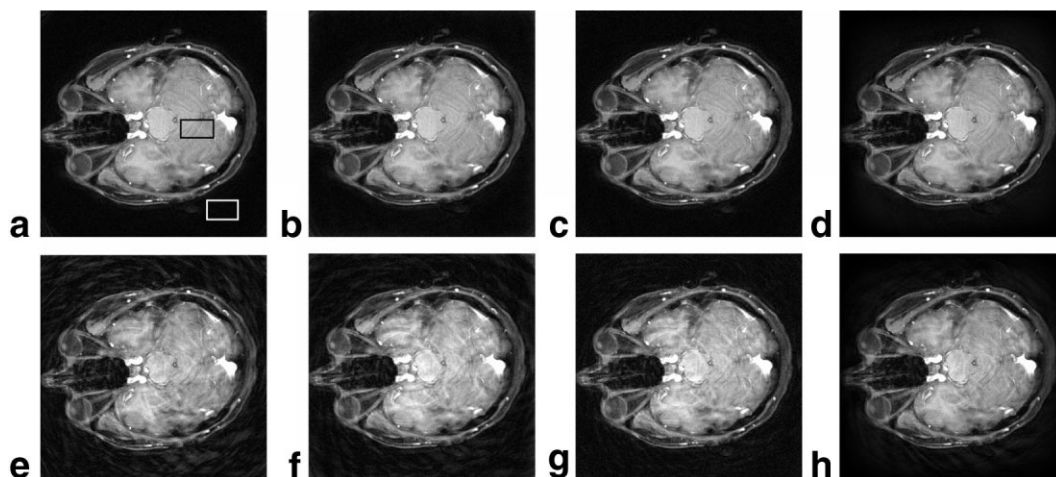


FIG. 9. Reconstructed in vivo brain images for the spiral trajectory using conventional gridding (a), F-CG without (b) and with the spiral DCF (c), and DING (d). Below are the images reconstructed from the irregular spiral that results from omission of every eighth interleave, using conventional gridding (e), and F-CG without (f) and with Voronoi DCF (g), and DING (h). Note the severe artifacts in e compared to f–h. The black and white rectangles denote regions inside and outside the object sampled for SNR measurements.

Lower RMS errors and comparable SNR are achieved using DING, as is evident from Tables 2 and 3. A lower SNR might be expected for DING, which involves a deconvolution process, as compared to the smoothing convolution operation of the conventional gridding algorithm. However, no significant SNR degradation is observed, which reflects the inherent regularization of the CG method. On the other hand, no artifacts are discernible in the DING-reconstructed images. This contrasts with the well-known wing artifact with conventional gridding if subsampling is not performed and/or sampling artifacts when irregular k -space sampling schemes are deployed.

One of the advantages of DING is that the problem of calculating the DCF can be completely avoided because density compensation is inherent in the deconvolution step. Avoiding the calculation of the DCF is an important property, especially when analytical solutions are unavailable, as is the case for the random trajectory we used, or when the trajectory crosses itself. The DCF is the major factor that determines the accuracy of the conventional gridding algorithm, and discrete approximation of the convolution operation is highly dependent on the DCF (3). Errors in density compensation are magnified by the aliasing and roll-off-correction processes. Significant artifacts in the reconstructed image may result if the sampling density is not rendered uniform after the DCF is applied. This is the case for the random trajectory in which the random sampling density is not efficiently compensated for, resulting in the artifacts in Fig. 6 compared to the artifact-free images for the spiral trajectory in Fig. 3. Unfortunately, the existence of a sufficiently good DCF for an arbitrary trajectory is not guaranteed, and in such situations DING provides a better solution. The improved performance of DING is essentially due to the accuracy of the deconvolution operation, and is largely independent of the sampling trajectory as long as the sampling rate is sufficient to avoid aliasing. This is evident in Fig. 6, which shows that the DING-reconstructed image is free of the

reconstruction artifacts present in the conventional gridding image.

The memory requirement for DING is the same as that for conventional gridding without grid subsampling, because the same gridding matrix is used. The reconstruction accuracy of DING is about the same as or better than that of conventional gridding with a twice-finer grid. Thus, there is about a fourfold saving in memory requirement for 2D trajectories, and the saving is even greater for 3D trajectories. The F-CG method has the same memory requirements as conventional gridding because F-CG uses conventional gridding to implement the matrix-vector multiplication in each CG iteration.

Both DING and F-CG have a higher computational load than the conventional gridding algorithm as a cost of their improved accuracy. In the following, we compare the computational load of the three reconstruction methods assuming comparable image quality. This requires implementing the conventional gridding algorithm with a twice-finer grid to avoid artifacts. Let J be the number of neighboring grid points around each of the trajectory samples. In the conventional gridding algorithm, reconstruction involves a single matrix-vector multiplication with a matrix size of $4N \times L$ with $4LJ$ nonzero elements. This is about four times the computational load required for a regular grid. The computational requirement of DING for a K -iteration solution is $(2K + 1)$ matrix-vector multiplications. The matrix size is $L \times N$ and contains LJ nonzero elements. The result is a $\{(2K + 1)/4\}$ -fold increase in the number of multiplications over conventional gridding. A satisfactory solution is usually obtained in less than 15 iterations for a zero initial solution, which means an increase in computational load by a factor of about 8. Although the F-CG method generally has a better convergence rate than DING and thus requires less iterations for a stable solution, it also performs more work in each iteration because it involves a forward and an inverse gridding operations. The gridding operations are usually performed

on a subsampled grid, which increases the computational load. For a twice-finer grid and a K -iterations solution, the cost is about $(2K + 1) \times 4LJ$ multiplications. Assuming that the F-CG requires about half the number of iterations as DING (Fig. 8), the net result is a speed-up by a factor of 2 in DING compared to F-CG.

Note that two matrix-vector multiplications are needed for each CG iteration if the normal equation matrix $C^T C$ is not computed in advance. If this matrix is computed in advance, the number of matrix-vector multiplications is cut by almost half, reducing the computation time to only fivefold that of conventional gridding. However, this increase in speed comes at the expense of an increased memory requirement to store the C matrix, as well as the $C^T C$ matrix. In this case the fourfold reduction in memory requirements for DING reduces to about twofold compared to conventional gridding. Also, the speed-up factor may not be exactly 2, because the $C^T C$ matrix contains more nonzero elements than the sparse matrix C . This trade-off between memory requirements and computational speed can be made according to resource availability. In simulations, the number of iterations needed to achieve a stable DING solution ranged from 8 to 15 using a zero initial solution; however, when a good initial solution is available the number of iterations can be greatly reduced, thus improving the speed. For example, this can be done in dynamic studies where the image in one frame can be used as the initial solution for the next frame. The reconstruction times for conventional gridding, F-CG, and DING with memory-saving and higher-speed versions, were on average 0.7, 18.4, 9.4, and 4.6 s, respectively, for a 256×256 grid in the simulated spiral experiment.

An important feature of DING, which is shared by conventional gridding and F-CG, is that reconstruction of the gridding matrix is simple and remains relatively fast. On the same machine, the gridding matrix for the simulated spiral trajectory with 32×4096 samples and a 256×256 Cartesian grid can be constructed in less than 1.7 min. This is a useful property for situations in which the k -space trajectory is not known a priori. For example, when there is patient motion during the scan, locations of the acquired samples are unknown until the motion is estimated. Rotational motion of the imaged object corresponds to a similar rotation of the k -space samples, resulting in an irregular sampling pattern. Computationally intensive techniques for constructing the gridding matrix (8) and the DCF (6) are unsuitable in such cases, whereas DING provides an easy way to construct the gridding matrix while avoiding density-compensation problems. Motion-correction schemes (27,28) may thus benefit from utilizing DING to efficiently suppress motion-induced blurring and improve the fidelity of the reconstructed image.

CONCLUSIONS

We have introduced DING as a new method for reconstructing images from arbitrarily sampled k -space. DING performs better than conventional gridding in terms of reconstruction accuracy and memory requirements, at some cost to reconstruction speed. Its performance is better than F-CG in terms of speed, memory, and noise suppression. Deconvolution-interpolation, as opposed to con-

volution-interpolation, is the underlying difference that yields the better accuracy in DING compared to conventional gridding. DING completely avoids the problem of calculating a DCF, since density compensation is inherent in the deconvolution process. Reconstruction of the gridding matrix is a simple and fast process, and thus provides flexibility for k -space trajectories that are often changed or not known a priori. The regularization inherent in the CG method helps to stabilize the performance of DING in the presence of noise.

ACKNOWLEDGMENTS

We thank Ronald Ouwerkerk and Abdel-Monem El-Sharkawy at Johns Hopkins University for helpful discussions and comments, and the anonymous journal referees whose input improved this work.

REFERENCES

- O'Sullivan JD. A fast sinc function gridding algorithm for Fourier inversion in computer tomography. *IEEE Trans Med Imaging* 1985;4:200–207.
- Jackson JJ, Meyer CH, Nishimura DG, Macovski A. Selection of a convolution function for Fourier inversion using gridding. *IEEE Trans Med Imaging* 1991;10:473–478.
- Schomberg H, Timmer J. The gridding method for image reconstruction by Fourier transformation. *IEEE Trans Med Imaging* 1995;14:596–607.
- Desplanques B, Cornelis J, Achten R, Walle RVD, Lemahieu I. Iterative reconstruction of magnetic resonance images from arbitrary samples in k -space. *IEEE Trans Nucl Sci* 2002;49:2268–2273.
- Walle RVD, Barrett HH, Myers KJ, Altbach MI, Desplanques B, Gmitro AF, Cornelis J, Lemahieu I. Reconstruction of MRI images from data acquired on a general non-regular grid by pseudoinverse calculation. *IEEE Trans Med Imaging* 2000;19:1160–1167.
- Pipe JG, Menon P. Sampling density compensation in MRI: rationale and an iterative numerical solution. *Magn Reson Med* 1999;41:179–186.
- Sedarat H, Nishimura DG. On the optimality of the gridding reconstruction algorithm. *IEEE Trans Med Imaging* 2000;19:306–317.
- Rosenfeld D. An optimal and efficient new gridding algorithm using singular value decomposition. *Magn Reson Med* 1998;40:14–23.
- Moriguchi H, Wendt M, Duerk JL. Applying the uniform resampling (URS) algorithm to a lissajous trajectory: fast image reconstruction with optimal gridding. *Magn Reson Med* 2000;44:766–781.
- Moriguchi H, Duerk JL. Modified block uniform resampling (BURS) algorithm using truncated singular value decomposition: fast accurate gridding with noise and artifact reduction. *Magn Reson Med* 2001;46:1189–1201.
- Rosenfeld D. New approach to gridding using regularization and estimation theory. *Magn Reson Med* 2002;48:193–202.
- Sutton BP, Fessler JA, Noll D. A min-max approach to the nonuniform N-D FFT for rapid iterative reconstruction of MR images. 2001. p 763.
- Sarty GE, Bennett R, Cox RW. Direct reconstruction of non-Cartesian k -space data using a nonuniform fast Fourier transform. *Magn Reson Med* 2001;45:908–915.
- Sha L, Guo H, Song AW. An improved gridding method for spiral MRI using nonuniform fast Fourier transform. *J Magn Reson* 2003;162:250–258.
- Sutton BP, Noll DC, Fessler JA. Fast, iterative image reconstruction for MRI in the presence of field inhomogeneities. *IEEE Trans Med Imaging* 2003;22:178–188.
- Fahmy AS, Tawfik B, Kadah YM. Gridding using optimal spatially variant kernel. In: *Proceedings of the 10th Annual Meeting of ISMRM*, Honolulu, HI, USA, 2002. p 2423.
- Rasche V, Proksa R, Sinkus R, Bornert P, Eggers H. Resampling of data between arbitrary grids using convolution interpolation. *IEEE Trans Med Imaging* 1999;18:385–392.

18. Pruessmann KP, Weiger M, Bornert P, Boesiger P. Advances in sensitivity encoding with arbitrary k-space trajectories. *Magn Reson Med* 2001;46:638-651.
19. Kadah YM, Fahmy A, Gabr R, Heberlein K, Hu X. Progressive magnetic resonance image reconstruction based on iterative solution of a sparse linear system. *Int J Biomed Imaging* 2006;2006:1-9.
20. Banham MR, Katsaggelos AK. Digital image restoration. *IEEE Signal Process* 1997;14:24-41.
21. Golub GH, Loan CFV. Matrix computations. Baltimore, MD: Johns Hopkins University Press; 1989.
22. King KF, Foo TK, Crawford CR. Optimized gradient waveforms for spiral scanning. *Magn Reson Med* 1995;34:156-160.
23. Moriguchi H, Duerk JL. Iterative next-neighbor regridding (INNG): improved reconstruction from nonuniformly sampled k-space data using rescaled matrices. *Magn Reson Med* 2004;51:343-352.
24. Hoge RD, Kwan RK, Pike GB. Density compensation functions for spiral MRI. *Magn Reson Med* 1997;38:117-128.
25. Firbank MJA, Coulthard RMH, Williams ED. A comparison of two methods for measuring the signal to noise ratio on MR images. *Phys Med Biol* 1999;44:N261-N264.
26. Tsai CM, Nishimura DG. Reduced aliasing artifacts using variable-density k-space sampling trajectories. *Magn Reson Med* 2000;43:452-458.
27. Ahmed HM, Gabr RE, Heberlein K, Hu X, Kadah YM. New strategy for simultaneous suppression of intra- and inter-slice motion. In: Proceedings of the 11th Annual Meeting of ISMRM, Toronto, Canada, 2003. p 1060.
28. Pipe JG. Motion correction with PROPELLER MRI: application to head motion and free-breathing cardiac imaging. *Magn Reson Med* 1999;42: 963-969.